Adenine radicals generated in alternating AT duplexes by direct absorption of low-energy UV radiation

Akos Banyasz, Tiia Ketola, Lara Martinez-Fernandez, Roberto Improta, Dimitra Markovitsi

Faraday Discussions

Cite this: *Faraday Discuss.*, 2018, **207**, 181

PAPER

Adenine radicals generated in alternating AT duplexes by direct absorption of low-energy UV radiation

Akos Banyasz,[a] Tiia Ketola,[a] Lara Martínez-Fernández,[b] Roberto Improta*[ab] and Dimitra Markovitsi*[a]

Received 24th July 2017, Accepted 12th September 2017
DOI: 10.1039/c7fd00179g

There is increasing evidence that the direct absorption of photons with energies that are lower than the ionization potential of nucleobases may result in oxidative damage to DNA. The present work, which combines nanosecond transient absorption spectroscopy and quantum mechanical calculations, studies this process in alternating adenine–thymine duplexes $(AT)_n$. We show that the one-photon ionization quantum yield of $(AT)_{10}$ at 266 nm (4.66 eV) is $(1.5 \pm 0.3) \times 10^{-3}$. According to our PCM/TD-DFT calculations carried out on model duplexes composed of two base pairs, $(AT)_1$ and $(TA)_1$, simultaneous base pairing and stacking does not induce important changes in the absorption spectra of the adenine radical cation and deprotonated radical. The adenine radicals, thus identified in the time-resolved spectra, disappear with a lifetime of 2.5 ms, giving rise to a reaction product that absorbs at 350 nm. In parallel, the fingerprint of reaction intermediates other than radicals, formed directly from singlet excited states and assigned to AT/TA dimers, is detected at shorter wavelengths. PCM/TD-DFT calculations are carried out to map the pathways leading to such species and to characterize their absorption spectra; we find that, in addition to the path leading to the well-known TA* photoproduct, an AT photo-dimerization path may be operative in duplexes.

Introduction

Low-energy UV radiation may damage DNA in an indirect or direct way. According to the former mechanism, photons are absorbed by molecules that are present close to the nucleic acids, which in turn react with DNA, thus modifying its chemical structure. In the case of direct damage, UV photons are absorbed by nucleobases, with the other components of nucleic acids being transparent in the

[a]*LIDYL, CEA, CNRS, Université Paris-Saclay, F-91191 Gif-sur-Yvette, France. E-mail: robimp@unina.it; dimitra.markovitsi@cea.fr*

[b]*Istituto Biostrutture e Bioimmagini – Consiglio Nazionale delle Ricerche, Via Mezzocannone 16, I-80134 Napoli, Italy*

spectral area. While it is well documented that cyclobutane pyrimidine dimers, the major UV-induced lesions in DNA, may be formed by either mechanism,[1] it is currently considered that oxidative damage is provoked exclusively in an indirect way.[2] The latter conclusion is proposed due to the high vertical ionization potential of nucleobases (>7 eV according to the most recent studies[3]), which is expected to render photo-ionization impossible at wavelengths corresponding to the lowest absorption band which peaks at around 260 nm (Fig. 1).

Surprisingly, a recent study reported the detection of a well-known oxidation marker, 8-oxo-7,8-dihydro-2′deoxyguanosine (8-oxoG) in purified naked genomic DNA irradiated at 254 and 300 nm.[4] More importantly, it was demonstrated that 8-oxoG does not result from reactions involving singlet oxygen, as had been postulated in the past,[5,6] but rather stems from guanine radical cations. This finding made a connection with older spectroscopic studies on short oligonucleotides, which observed electron ejection following UV excitation at wavelengths ranging from 260 to 300 nm.[7–9]

A quantitative characterization of both the ejected electrons and the resulting nucleobase radicals as a function of the base sequence is an important step towards understanding one-photon ionization of DNA by low-energy UV radiation. To this end, a tool of choice is nanosecond absorption spectroscopy, which is already used to study one-photon ionization of bases, nucleosides and nucleotides at 193 nm.[10] Photo-ejected electrons are rapidly hydrated, giving rise to a broad absorption band at around 700 nm,[11] which is detectable on the sub-microsecond time-scale.[7,12] Despite the apparent facility of such measurements, a series of obstacles must be overcome in order to properly characterize these transient species. (i) The excitation intensity should be reduced so as to avoid two-photon ionization of the aqueous solvent and minimize two-photon ionization of DNA. However, the drawback of this is the production of very weak optical signals. (ii) Reactions of ejected electrons with the studied system should be prevented; hydrated electrons are known to attack nucleic acids, forming electron adducts which absorb in the same spectral domain as radicals stemming from photo-ionization.[10,12,13] (iii) The transient absorption spectra associated with photo-ionization should be disentangled from those arising from UV-induced base dimerization reactions.[14,15]

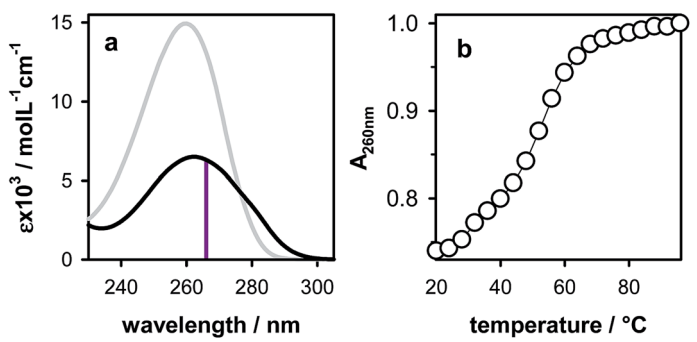

Fig. 1 (a) Absorption spectra of $(AT)_{10}$ (black) and dAMP (grey); (b) typical melting curve obtained for $(AT)_{10}$. The violet line indicates the excitation wavelength, 266 nm, that was used in transient absorption experiments.

In addition to these experimental difficulties, the effect of the duplex on the radical spectra has never been fully disclosed. Their assignment is based on their similarity with the corresponding mononucleotide spectra.[8,16] On the other hand, radical cations $(A)^{+\bullet}$ and deprotonated radicals $(A\text{-}H6)^{\bullet}$, from which a proton has been abstracted from the position 6 of adenine, have similar spectra,[17] thus rendering their assignment in duplexes not straightforward.

Within this general context, we have recently undertaken an investigation of one-photon ionization of model DNA multimers at 266 nm by controlling the aforementioned experimental problems and combining time-resolved absorption experiments with quantum mechanical calculations. Thus, we determined the spectral and dynamical features of adenine radicals in A-tracts[17] and identified the reaction intermediate leading to adenine dimerization.[15] Moreover, we reported the first UV-induced oxidation study of G-quadruplexes.[18]

The present work focuses on alternating adenine–thymine $(AT)_n$ double-stranded structures. Such structures correspond to the so called TATA boxes encountered in the human genome, which play a crucial role in gene transcription.[19] Experimentally, we study duplexes with 20 base pairs, abbreviated as $(AT)_{10}$, using transient absorption spectroscopy with excitation at 266 nm, near the absorption maximum (Fig. 1a). Ejected electrons are quantified with a time-resolution of 30 ns and disappear without interacting with the duplexes. Subsequently, we follow the fate of adenine radicals. In parallel, we detect the fingerprints of the dimerization reactions. Such reactions are known to occur on the singlet excited state following 254 nm excitation of AT strands,[20–23] leading to the formation of various photoproducts whose nature is still a matter of debate.[24]

Our experimental results are interpreted in the light of quantum mechanical calculations (TD-DFT). As the structural arrangement of the bases in $(AT)_n$ duplexes may be different for the AT and TA steps,[25] we studied both sequences, using the two model duplexes $(AT)_1$ and $(TA)_1$ shown in Fig. 2. We provide the absorption spectra of the base radicals within these duplexes. Moreover, following a preliminary study on single stranded dinucleotides,[26] we map, for the first time, different reaction paths leading to adenine–thymine dimerization within double-stranded structures and compute the absorption spectra of the main reaction intermediates.

Methodological details

Spectroscopic setups

Steady-state absorption spectra were recorded using a Lambda 900 (Perkin-Elmer) spectrophotometer.

Time-resolved experiments were performed using a home-made nanosecond flash photolysis setup. The excitation source was the fourth harmonic of a Nd:YAG laser (Spectra-Physics, Quanta Ray) and the excitation frequency was 0.2 Hz. The energy of the exciting pulse was measured using a NIST traceable pyroelectric sensor (OPHIR Nova2/PE25). The excited area at the surface of the sample was 0.06 cm^2, with the optical path-length on the excitation side being 0.1 cm.

The analysing beam (150 W Xe-arc lamp, Applied Photophysics) passed through the sample (optical length 1 cm) at a right angle with respect to the exciting beam, was dispersed in a SPEX 270M monochromator and detected by a Hamamatsu R928 photomultiplier. The signal from the photomultiplier was

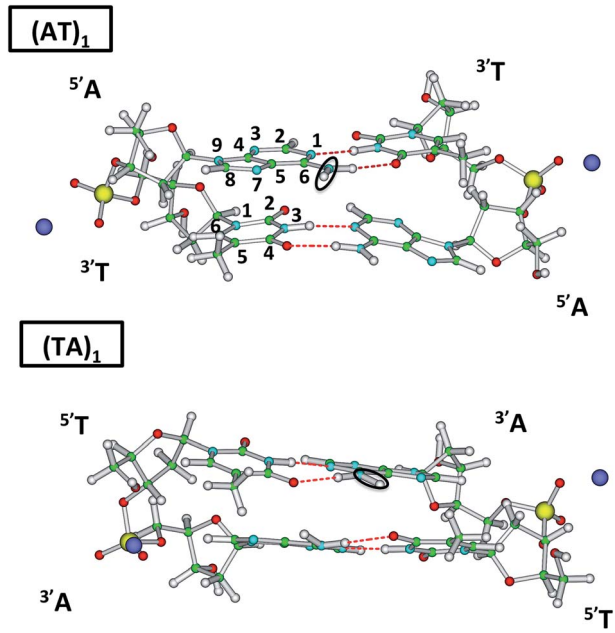

Fig. 2 Schematic drawing of the two computational models, denoted by $(AT)_1$ and $(TA)_1$, used to account for AT and TA steps in double-stranded structures. The black frames highlight the positions where deprotonation occurs.

recorded using a Lecroy Waverunner 6050 oscilloscope. Detection on the sub-microsecond time-scale was achieved by intensifying the emission intensity of the Xe-arc lamp *via* an electric discharge. Transient absorption spectra were recorded using a wavelength-by-wavelength approach. Typically, at each wavelength, a series of three successive signals, resulting from 50–150 laser shots each, were recorded; if judged to be reproducible they were averaged to increase the signal-to-noise ratio.

Fast shutters were placed in the path of both the laser and lamp beams in order to minimize sample exposure to both light sources.

Oligonucleotide handling

Oligonucleotides were purchased from Eurogentec Europe; they were purified by HPLC and their quality was tested by carrying out MALDI-TOF measurements. They were dissolved in phosphate buffer (0.15 mol L^{-1} NaH_2PO_4, 0.15 mol L^{-1} Na_2HPO_4) using ultrapure water delivered by a MILLIPORE (Milli-Q Synthesis) system. The pH of the buffer solutions was adjusted to 7 by addition of a concentrated NaOH solution. The duplexes were prepared in a dry bath (Eppendorf-ThermoStatplus); 2 mL of concentrated oligomer solution was heated to 96 °C for 5 min, then cooled to the melting point (cooling time: 1 h), where the temperature was maintained for a few minutes; subsequently, the solution was cooled to 4 °C (cooling time: 2 h) and incubated overnight. A typical melting curve is shown in Fig. 1b.

For the detection of hydrated electrons on the sub-μs scale, 2 mL of solution, contained in a 1 cm × 1 cm quartz cell, was argon saturated and mildly stirred

during the experiment; fresh samples were used for each excitation intensity. For recording transient signals at longer times, both quartz cells containing 3 mL of solution and a flow system allowing the circulation of 40 mL of solution were used. In all cases, the optical density on the excitation side was 0.25 ± 0.02 over 0.1 cm, corresponding to a duplex concentration of 9.6×10^{-5} mol L^{-1}. At the maximum excitation intensity (3.3 MW cm^{-2}), the concentration of ejected electrons was 1.2×10^{-6} mol L^{-1}, which was significantly lower than the duplex concentration.

During the experiments the temperature was maintained at 23 ± 0.5 °C.

Theoretical methods

The starting geometry of our model duplexes was taken from the X-ray structure 1DN9.pdb,[25] in which the AT and TA steps exhibit different stacking arrangements, with the former showing much better overlap between bases. The ground state minima of the $(AT)_1$ and $(TA)_1$ dimers, their radical species, and possible intermediates and photoproducts were optimized using Density Functional Theory (DFT). The selected functional was M052X,[27,28] due to its good performance for treating stacked systems, and was combined with the 6-31G(d) basis set. The Polarizable Continuum Model (PCM) was used to account for solvent (water) effects.[29,30] We exploited the time dependent version of DFT (TD-DFT) to compute the absorption spectra at the ground state minima and to characterize their excited state Potential Energy Surfaces (PESs). This computational approach has provided satisfactory results in previous studies both for radical spectra[17,18] and for photo-dimerization processes.[15,26,31–33] For a better comparison with the experimental absorption spectra, the computed Vertical Excitation Energies (VAE) were red-shifted by 0.6 eV and convoluted using a Gaussian with a full width at half maximum (fwhm) of 0.6 eV. The applied shift allows the VAE computed for the lowest bright $\pi\pi^*$ excited state of adenine at this level of theory to coincide with the experimental maximum of the absorption band; this accounts for the absence of vibronic and thermal effects, besides the possible inaccuracies of our electronic calculations.

Results and discussion

The photo-ionization process

Fig. 3a shows the signal of the hydrated electron obtained for an argon saturated $(AT)_{10}$ solution and the aqueous buffered solvent alone at the maximum excitation intensity. As the solvent signal is practically flat, we can conclude that the decay observed for the $(AT)_{10}$ solution corresponds to electrons stemming only from the duplex. The decay can be fitted with a single exponential function $c + \Delta A_0 \exp(-t/\tau)$ with a time constant of 0.42 μs. This value is independent of the base sequence[17,18] and is also found for the solvent alone at much higher excitation intensities, thus showing that hydrated electrons do not react with the duplex; they are scavenged by the phosphate groups[34] of the buffer at high concentration. The initial concentration of hydrated electrons $[e]_0$ is determined from the ΔA_0 value and the most recent value reported for their molar absorption coefficient (19 700 mol L^{-1} cm^{-1} at 700 nm).[11]

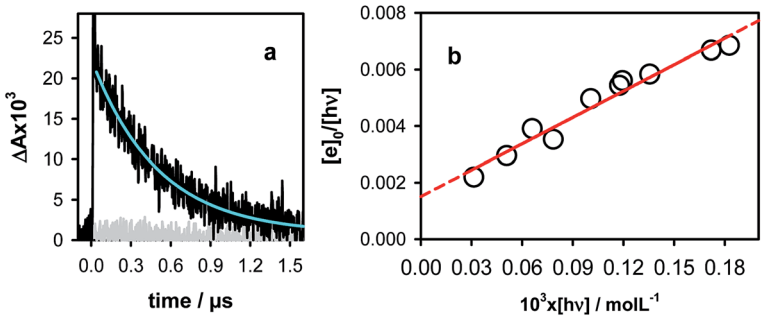

Fig. 3 (a) Transient absorption decay recorded for an argon saturated $(AT)_{10}$ solution at 700 nm (black) fitted with a mono-exponential function (cyan); in grey is the signal obtained for the solvent at the same excitation intensity of 3.3 MW cm^{-2}. (b) Ionization curve of $(AT)_{10}$ obtained by varying the excitation energy; [hν] and $[e]_0$ denote the concentrations of absorbed photons and hydrated electrons at time zero, respectively; the experimental points (circles) are fitted with a linear function (red line).

Although one-photon ionization is the biologically relevant process, laser experiments also provoke two-photon ionization of duplexes. This is probably due to absorption of a second photon during the 5 ns laser pulse by long-lived singlet excited states, charge transfer (CT) states whose lifetimes amount to tens of ps,[35,36] and high energy long-lived mixed (HELM) states surviving on the ns time-scale.[37] The electron concentration $[e]_0$ varies as a function of the concentration of absorbed photons [hν] according to the equation $[e]_0 = \phi_{1h\nu}[h\nu]_{1hn} + \phi_{2hn}[h\nu]^2$, where $\phi_{1h\nu}$ and $\phi_{2h\nu}$ represent, respectively, the yields of the one- and two-photon processes. While the quantum yield $\phi_{1h\nu}$ corresponds to an intrinsic property of the duplex, $\phi_{2h\nu}$ depends also on the experimental conditions.[38]

The so-called ionization curve is obtained by plotting $[e]_0/[h\nu]$ *versus* [hν] and fitting the experimental points with a linear function (Fig. 3b). The slope of the fitted line corresponds to two-photon ionization and the intercept on the vertical axis provides the one-photon ionization quantum yield, $(1.5 \pm 0.3) \times 10^{-3}$. The $\phi_{1h\nu}$ value determined from the plot in Fig. 3b is higher than that derived from previous measurements, such as $(1.0 \pm 0.1) \times 10^{-3}$ which was obtained with a time resolution of 200 ns;[8] we note that, for better comparison, the 2006 $\phi_{1h\nu}$ value was re-evaluated using the molar absorption coefficient (19 700 mol L^{-1} cm^{-1}) reported in 2016.[11] Following a similar re-evaluation, the $\phi_{1h\nu}$ value of the homopolymeric duplex was found to be $(1.3 \pm 0.3) \times 10^{-3}$. Consequently, we can conclude that the one-photon ionization of AT duplexes is not significantly affected by the base sequence.

We note that under the same experimental conditions, using excitation intensities of up to 3.3 MW cm^{-2}, we did not detect any hydrated electrons for neither dA nor dAMP.

Radical spectra in duplexes

The shapes of the spectra recorded for $(AT)_{10}$ between 2 μs, when hydrated electrons have already disappeared, and 0.2 ms do not exhibit any noticeable difference. The spectrum at 0.2 ms is presented in Fig. 4a. It is composed of two bands

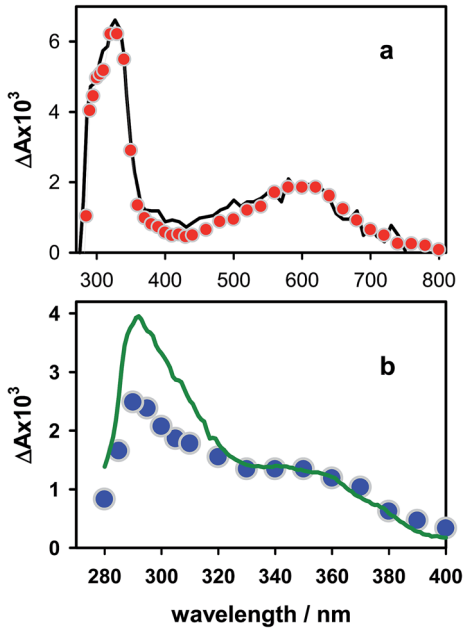

Fig. 4 Time-resolved absorption spectra obtained for an aerated solution of $(AT)_{10}$ at 0.2 ms ((a), red) and 30 ms ((b), blue). Excitation intensity: 3.3 MW cm^{-2}. The black line in (a) corresponds to the spectrum of the deprotonated radical $(A\text{-}H6)^{\bullet}$ determined for dAMP,[13] normalized at 600 nm with the duplex spectrum. The green line in (b) corresponds to the difference between the steady-state spectra of $(AT)_{10}$ recorded before and immediately after irradiation with 200 laser pulses, normalized with the spectrum at 30 ms at 350 nm.

that peak at around 330 and 600 nm. At 30 ms the 600 nm band has disappeared but absorption still persists below 400 nm, characterized by a peak at 300 nm and a shoulder at 350 nm (Fig. 4b). Its origin will be discussed later.

The $(AT)_{10}$ spectrum at 0.2 ms strongly resembles that obtained for dAMP at 300 ns following excitation at 193 nm,[13] also shown in Fig. 4a, which is attributed to the deprotonated adenine radical $(A\text{-}H6)^{\bullet}$. The latter attribution was recently confirmed by comparing the spectra of the dA radical cation and deprotonated radical in low temperature glasses, with the spectra of these transient species calculated using quantum chemistry methods.[17] This is also in agreement with pulse radiolysis studies which report that deprotonation takes place with a time constant of 50 ns.[39] However, in the case of UV-induced processes, the radical reactivity could be different from that reported in pulse radiolysis studies using two-step oxidation of bases and involving bimolecular electron transfer.[39] As a matter of fact, we recently showed[18] that the behaviour of guanine radical cations produced by photo-ionization in G-quadruplexes is not the same as that found for photo-sensitized processes in these systems.[40] Moreover, the similarity between the time-resolved differential spectra of $(AT)_{10}$ and that of the dAMP deprotonated radical observed in Fig. 4a could be fortuitous. This is particularly probable for the blue side of the transient spectrum corresponding to the difference between the radical spectrum and the ground state spectrum (Fig. 1a). As was found for adenine single strands[17] and G-quadruplexes,[18] this part of the

differential spectrum is different than that of the corresponding monomer because of the modification of the ground state spectrum due to delocalization of the Frank–Condon excited states over a few bases.[37,41] Finally, the dimeric photoproduct reported by Davies (denoted by TA*),[20] absorbs in the 270–320 nm region. Therefore, we computed the electronic transitions of the radical cations and deprotonated radicals for our two model double stranded structures $(AT)_1$ and $(TA)_1$ (Fig. 2) using the PCM/TD-M052X/6-31G(d)//M052X/6-31G(d) level of theory.

In Fig. 5 we present the spectra obtained for the radical cation $(AT)_1^{+\bullet}$ and the deprotonated radical $[(AT)_1\text{-H6}]^{\bullet}$, together with their monomeric counterparts computed at the same level of theory. We remark that the inclusion of the adenine radical within the double-stranded structure does not induce any drastic modification in the radical spectra. The positions and relative intensities of the peaks in the UV and visible spectral domains remain practically unchanged. This result is consistent with our prediction that for both $(AT)_1$ and $(TA)_1$ the positive charge is essentially localized on a single base. Yet, the oscillator strength is slightly higher compared to that of the monomer, and a larger number of electronic transitions, albeit extremely weak, are present in the 300–900 nm range. In particular, for the cation, three additional transitions are located at wavelengths longer than 750 nm; they involve interbase $\pi\pi^*$ excitations between the adenine bearing the positive charge and other bases, thus giving rise to a slightly more intense red tail in the spectrum. Analogously, several series of interbase $n\pi^*$ dark excited states, involving transitions from the lone pairs of other bases to the positively charged adenine, fall between the 300 and 600 nm bands. As the radical localization is more pronounced for $[(AT)_1\text{-H6}]^{\bullet}$ compared to that of the cation, the similarity of its spectrum with that of the monomer is greater. However, some additional interbase $\pi\pi^*$ transitions still arise in $[(AT)_1\text{-H6}]^{\bullet}$ at 480–520 nm, which is higher in energy in comparison with $(AT)_1^{+\bullet}$.

The features computed for our second model double-stranded structure $(TA)_1$ (Fig. 6) are quite similar to those shown in Fig. 5. As for $(AT)_1$, the relative intensities of the bands in the UV and visible regions are not altered with respect to those of the monomeric radicals. The differential $((TA)_1^{+\bullet}\text{–}(TA)_1$ and $[(TA)_1\text{-6H}]^{\bullet}\text{–}(TA)_1)$ absorption spectra computed for the $(TA)_1$ radicals are presented in Fig. 6.

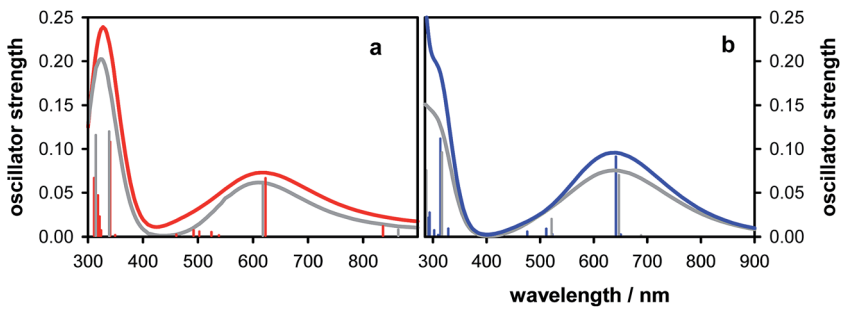

Fig. 5 Absorption spectra computed for the $(AT)_1^{+\bullet}$ radical cation ((a), red) and the $[(AT)_1\text{-6H}]^{\bullet}$ deprotonated radical ((b), blue). The corresponding spectra of 9-methyl-adenine are shown in grey. The sticks represent individual electronic transitions. Calculated at the PCM/TD-M052X/6-31G(d)//M052X/6-31G(d) level of theory.

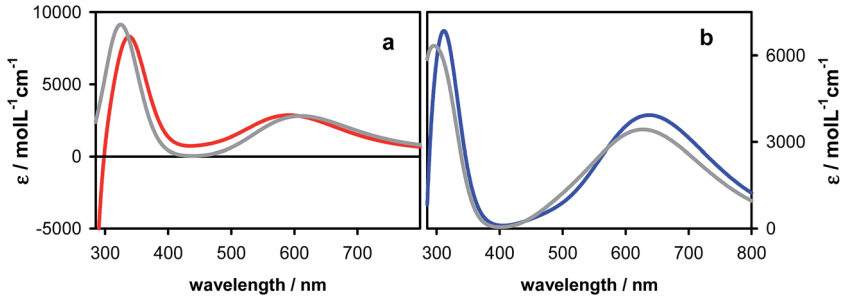

Fig. 6 Differential absorption spectra computed by subtracting the $(TA)_1$ absorption spectrum from the spectrum of the radical cation $(TA)_1^{+\bullet}$ ((a), red) and the deprotonated radical $[(TA)_1\text{-}6H]^{\bullet}$ ((b), blue). The corresponding spectra of 9-methyl-adenine are shown in grey. Calculated at the PCM/TD-M052X/6-31G(d)//M052X/6-31G(d) level of theory.

In the light of the computed spectra, it appears that deprotonation of the radical cation in the double stranded structures is expected to induce an increase in the transient absorbance. It is also clear that the UV peaks of both radicals in the duplexes are red-shifted compared to those of the corresponding monomeric radicals. Thus, the apparent similarity of the $(AT)_{10}$ spectrum at 0.2 ms to that of the monomeric $(A\text{-}H6)^{\bullet}$ (Fig. 4a) indicates the presence of other absorbing species. Below we explore these aspects in more detail.

Radical dynamics

The time-dependence of the transient absorption signal at 600 nm is shown in Fig. 7. No rise is observed after 2 μs, which is the shortest time at which the radical transient spectra were recorded. This observation, together with the lack of a pronounced red tail in the 2 μs spectrum of $(AT)_{10}$ compared to that of the monomer (Fig. 4a), confirms that, at the probed time-scale, we observe deprotonated radicals. The signal decays on the ms time-scale and can be fitted with a mono-exponential function with a time constant of 2.5 ms. The same time constant is found upon reducing the incident excitation intensity so as to increase the ratio of electrons ejected *via* one-photon ionization *versus* those resulting from two-photon ionization from 0.31 to 0.71. This shows that the radical decay does not depend on the mode of their formation.

Our study on A-tracts reported that base pairing increases the survival probability of the deprotonated adenyl radical.[17] Our present work corroborates this conclusion and shows that not only base pairing but also the base sequence affects the reactivity of this radical; its half time in the alternating duplex $(AT)_{10}$ (2.0 ± 0.1 ms) is clearly shorter than that in the homopolymeric duplex with the same number of base pairs (4 ± 1 ms), but significantly longer than that found for adenine single strands (1.0 ± 0.1 ms). One possible reason for this difference could be the increased rigidity of the homopolymeric duplex, as suggested by molecular dynamics simulations.[42] Another way to reduce the amplitude of conformational motions in the duplex is to decrease the temperature of the aqueous solution. We indeed found that lowering the temperature from 23° to 5 °C lengthens the radical lifetime (Fig. 7b) and increases the initial radical concentration by about 25%. In contrast, argon saturation of the solutions has no

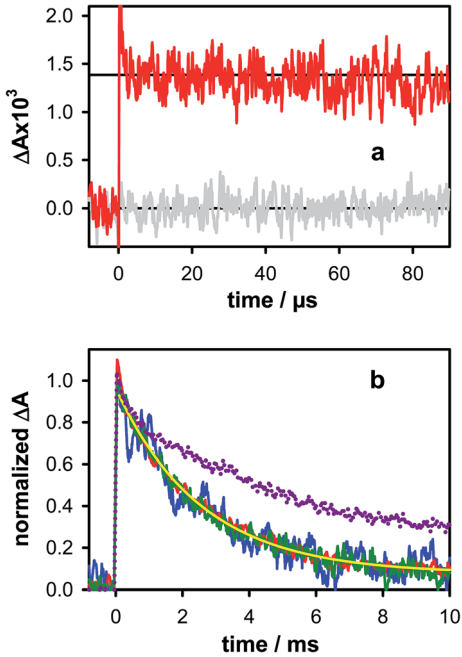

Fig. 7 Transient absorption signals recorded for $(AT)_{10}$ at 600 nm under different experimental conditions: solid lines (23 °C), dots (5 °C); the red, green and blue lines correspond, respectively, to $\phi_{1h\nu}/\phi_{2h\nu}$ ratios of 0.31, 0.63 and 0.71. (a) In grey: the signal of the buffer obtained under the same excitation intensity of 3.3 MW cm^{-2}. (b) In yellow: the fitted mono-exponential function with a time constant of 2.5 ms.

effect on the transient signals. This observation is in line with literature reports that monomeric adenyl radicals do not react with oxygen.[43]

The initial concentration of deprotonated radicals in $(AT)_{10}$ was evaluated using the differential absorbance determined at 2 μs (see an example in Fig. 7a) and the molar absorption coefficient reported for the dAMP deprotonated radical by Candeias and Steenken (1460 mol L^{-1} cm^{-1} at 600 nm). It was found to be 10% higher than the initial concentration of hydrated electrons determined for the same excitation intensity. This difference could either be due to the 10% estimated experimental error or reflect the fact the molar absorption coefficient of the deprotonated radical in double-stranded structures is higher than that of the monomeric analogue (Fig. 5 and 6).

UV-induced absorption below 400 nm

In order to discover the possible contribution of transient species other than adenine radicals to the early time spectra of $(AT)_{10}$ (Fig. 4a), we plotted in Fig. 8 typical transient absorption signals recorded at short wavelengths. All of them contain a plateau that appears at 20–30 ms and persists, at least, until 180 ms, which is the longest time that we can probe under these experimental conditions. We remark that, going from 330 nm to 280 nm, the pattern of the transient signal changes dramatically. The signals below 290 nm exhibit complex kinetics, being composed of a decay followed by a rise. An attempt to make a global fit with two

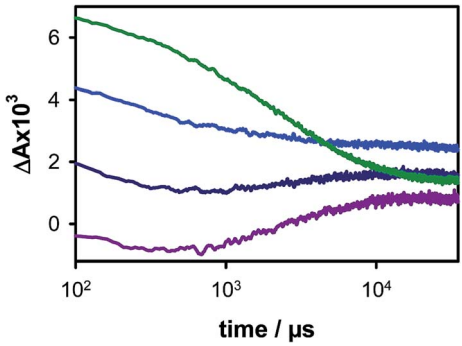

Fig. 8 Transient absorption signals recorded for $(AT)_{10}$ at 280 nm (violet), 285 nm (dark blue), 290 nm (blue) and 330 nm (green); excitation intensity 3.3 MW cm^{-2}.

exponential functions failed, thus indicating the presence of more than two species. Considering the absorption spectra computed for the duplex radicals (Fig. 5b and 6b) and the experimental transient absorption signals in Fig. 8, we can deduce that the UV part of the $(AT)_{10}$ spectra in Fig. 4 contains contributions from reaction intermediates other than radicals and/or their reaction products.

According to the literature, the TA* photoproduct, detected by Davies and identified as diazacyclooctatriene (see below), absorbs in the 280–330 nm region;[20–22,44,45] it is formed in the singlet excited state *via* a reaction intermediate, denoted hereafter as TA*–CB, because of the presence of a cyclobutane ring.[23] The relative concentration of TA*/TA*–CB *versus* that of the adenine radicals is expected to increase at low excitation intensities, for which two-photon ionization is less important (Fig. 3). We found indeed that when the excitation intensity decreases from 3.2 to 1.4 MW cm^{-2}, the intensity ratio of the 300 and 350 nm signals I_{300}/I_{350} increases from 1.7 to 2.0 at 0.2 ms and from 1.2 to 3.0 at 30 ms. This indicates that the absorption of reaction products resulting from the radicals is more intense at 350 nm compared to at 300 nm.

As a second step, we recorded steady-state absorption spectra for the $(AT)_{10}$ solutions before and after their irradiation with laser pulses. A different laser intensity was used for each sample and the number of laser pulses was adjusted so that the accumulated quantity of ejected hydrated electrons per volume to be the same for all the solutions, corresponding to a concentration of 1.7×10^{-6} mol L^{-1}, was the same for all of the solutions. The resulting steady-state differential spectra are shown in Fig. 9a. Despite the important noise due to the small amplitude of the signals, we clearly observe a peak around 295–300 nm, whose intensity increases linearly with the number of absorbed photons (Fig. 9b). In addition, a shoulder is present at around 350 nm, its intensity being roughly the same for all of the samples. Therefore, it appears that the radical reaction products are dominant at this wavelength. Interestingly, the time resolved spectrum at 30 ms also presents a shoulder at 350 nm (Fig. 4b).

From the slope of the linear regression in Fig. 9 we can deduce the equation $\Sigma\Delta\varepsilon_S \times \phi_S = 10.4$, where $\Delta\varepsilon_S$ and ϕ_S represent, respectively, the differential molar absorption coefficients and quantum yields corresponding to the various reaction products formed in the singlet excited state. Considering only the formation of

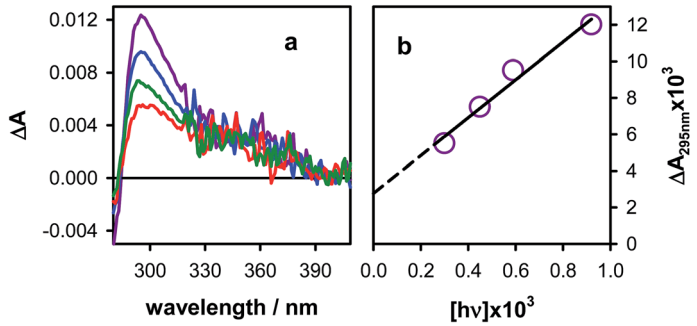

Fig. 9 (a) Steady-state differential absorption spectra obtained for different solutions of $(AT)_{10}$ irradiated by 266 nm laser pulses with intensities of 0.7 MW cm^{-2} (violet), 1.4 MW cm^{-2} (blue), 2.7 MW cm^{-2} (green) and 3.4 MW cm^{-2} (red). The total number of pulses per solution was adjusted so that the accumulated quantity of ejected electrons remained the same. (b) Variation of the maximum differential absorbance at 295 nm (a) as a function of the total concentration of absorbed photons (circles) fitted with a linear function (black line).

TA*, whose quantum yield in the $(AT)_n$ duplexes is *ca.* 10^{-4},[21] a $\Delta\varepsilon_S$ of 10^5 was found. Such a high value, encountered for strongly conjugated systems, has never been found for nucleobase derivatives. This indicates that absorption at 295 nm is due not only to TA*, but also to other photoproducts formed with a higher quantum yield, which is in line with what has been reported for adenine–thymine adducts in calf thymus DNA.[24] However, a comparison of the transient spectrum at 30 ms with the steady-state differential spectrum (Fig. 4b) shows that, for the latter spectrum, the relative intensity of I_{300}/I_{350} is higher. These observations suggest that the chemical species present in the solution evolve within the two hours that are needed to carry out the irradiation and obtain the steady-state spectrum shown in Fig. 4a, which is in line with what is reported in ref. 24.

Base dimerization in duplexes: computational approach

In this section, we first examine the reaction pathways (Fig. 10) of the singlet excited states of our two model duplexes (Fig. 2). We then compute the differential absorption spectra (Fig. 11) of the reaction intermediates, so that we can compare them with our experimental results.

Reaction paths in $(AT)_1$ duplexes. Confirming the results of previous QM studies on $(AT)_1$ model duplexes,[37] the lowest energy excited state in the ground state geometry derives from the interaction of $\pi\pi^*$ states localized on thymines (which are the dominant component) with the A $\rightarrow$ T charge transfer (CT) state. The partial CT character increases following geometry optimization of S_1, leading to a minimum, (AT_1)-S_1-min, where the two bases are very close to each other. The distance of C4A–C6T is 2.6 Å and the LUMO orbital involved in the S_1 transition exhibits a significant bonding contribution between these two atoms (Fig. 10). A relaxed scan that decreases this distance indeed shows that an almost barrierless path (barrier $\leq$ 0.1 eV) connects the $(AT)_1$-S_1-min to a degeneracy region with S_0. This region is characterized by a C4A–C6T distance of 2.00 Å. Subsequent S_0 geometry optimization leads to a stable minimum, whose energy is only 1.81 eV

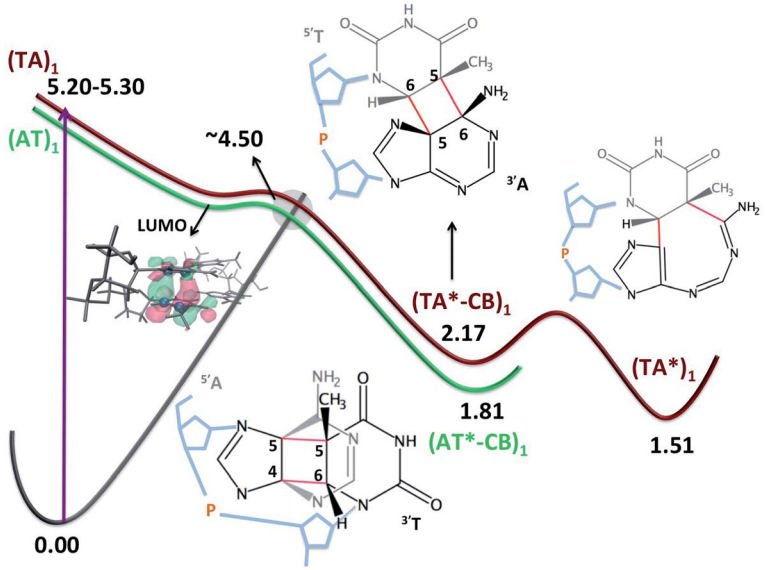

Fig. 10 Excited state pathways and schematic representation of the reaction intermediates (for simplicity we show only the strand involved in photo-dimerization) computed for $(AT)_1$ (green) and $(TA)_1$ (dark red). The energies (in eV) are given with respect to the ground state at the Franck–Condon point.

above the $(AT)_1$-S_0-min (Fig. 10). At this ground state minimum, C5A–C5T are also bonded, producing a cyclobutyl-like photo-adduct $(AT^*–CB)_1$. On the other hand, State-Specific (SS)-PCM/TD-M052X calculations (which provide a more reliable description of electronic transitions with CT character)[46] on dApT indicate that full equilibration of the solvent degrees of freedom leads to the appearance of a sizeable energy barrier (~0.5 eV) in the path connecting the $(AT)_1$-S_1-min and the crossing region.[26] Dynamical solvation effects should be less important inside the duplex. Nonetheless, we expect that our estimate of the energy barrier (≤0.1 eV) is a lower bound to the effective one in the duplex.

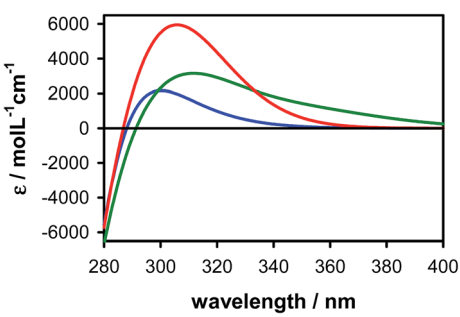

Fig. 11 Computed differential absorption spectra for $(AT^*–CB)_1$ (blue), $(TA^*–CB)_1$ (green) and $(TA^*)_1$ (red). Calculated at the PCM/TD-M052X/6-31G(d)//M052X/6-31G(d) level of theory.

Reaction paths in $(TA)_1$ duplexes. As discussed above, bases are poorly stacked in the TA steps compared to the AT steps. Consequently, S_1 geometry optimization, starting from the ground state minimum $(TA)_1$-S_0-min, predicts the localization of the excitation on a single T base. In order to study the photochemical paths, we have thus first optimized the 'Davies-like' photo-adduct, $(TA^*–CB)_1$, and then, by increasing the C6A–C5T distance, located the excited state minimum related to this $(TA)_1$-S_1-min adduct. $(TA^*–CB)_1$ is significantly less stable than $(AT^*–CB)_1$ and $(TA)_1$-S_1-min less stable than $(AT)_1$-S_1-min. On the other hand, a more stable minimum can be reached from $(TA^*–CB)_1$, corresponding to $(TA^*)_1$, the 1,3-diazacyclooctatriene product isolated for TpdA.[23]

Our calculations thus confirm the possibility of producing the Davies adduct in the duplexes. In addition, we show that, due to the geometry of the TA steps in the duplexes, this path is less effective than in single strands, thus accounting for the decreased TA* yield in the duplexes.[21,24] Moreover, the photochemical path leading to $(AT^*–CB)_1$, involving the AT steps, is favoured over that leading to $(TA^*–CB)_1$. On this ground, we propose that $(AT^*–CB)_1$ is the precursor of the hydration product found to be the most abundant "adenine–thymine" photoproduct in calf thymus DNA.[24]

Absorption spectra of reaction intermediates. We have computed the absorption spectra associated with the three species $(AT^*–CB)_1$, $(TA^*–CB)_1$ and $(TA^*)_1$ located along the potential energy surfaces in Fig. 10. The corresponding differential spectra, derived by subtracting the ground state absorption, are presented in Fig. 11. They peak, respectively, at 300, 311 and 306 nm. Considering the possible inaccuracies of our method and the use of smaller molecular models, all three spectra could be consistent with the transient spectra recorded for $(AT)_{10}$. On the other hand, it should be noted that, due to the peak position and the lack of absorption above 330 nm, the $(AT^*–CB)_1$ spectrum is the closest match to the transient spectrum at 30 ms (Fig. 4b), thus supporting our suggestion that it plays a major role in the photo-dimerization pathways.

The spectra in Fig. 11 allow us to roughly estimate the quantum yield for the formation of dimeric photoproducts. Using an average value of 2500 mol L^{-1} cm^{-1} for the differential molar absorption coefficient at 295 nm, corresponding to the three compounds in Fig. 11, and the equation $\Sigma\Delta\varepsilon_S \times \phi_S = 10.4$ derived from Fig. 9b, we find that the average quantum yield amounts to 4×10^{-3}. The latter value is of the same order of magnitude as that determined for radical formation, thus showing that the probability of base dimerization and oxidative damage is similar at 266 nm. Hopefully, future experiments will determine how these reaction paths vary with the irradiation wavelength.

Conclusions and outlook

The present study on alternating $(AT)_n$ duplexes, combining nanosecond laser photolysis and quantum mechanical calculations, presents new insights, not only into photo-ionization but also into the UV-induced base dimerization processes in these systems. Below, we summarize the main results and highlight open questions that might invite further research.

Our work shows that the direct absorption of single photons at 266 nm with energies that are 3.0 eV lower than the adenine ionization potential (7.7 eV)[3] leads to electron ejection, thus confirming the finding of an older study.[8] The one-

photon ionization yield ($1.5 \pm 0.3 \times 10^{-3}$), determined with the improved experimental setup used in the present work (time-resolution of 30 ns instead of 200 ns, lower excitation intensity by a factor of 2), is 50% higher than that of the first observation reported a decade ago. Under the same experimental conditions, a quantum yield of $(1.3 \pm 0.3) \times 10^{-3}$ was found for the homopolymeric analogue.[17] It appears that, within the current experimental errors, the one-photon ionization of adenine–thymine duplexes is not significantly affected by the base sequence. The mechanism of electron ejection resulting from the absorption of low-energy photons remains to be discovered. We can speculate that the CT states, which have been shown to be formed in significant yield in AT duplexes,[36,47] are the gateway for electron ejection.

Our calculations show that inclusion of the adenine radical cation and deprotonated adenine radical within double-stranded structures does not induce large modifications in their absorption spectra but does affect the differential absorption spectra because of the collective nature of the Frank–Condon excited states of the "neutral" species. In light of these theoretical predictions, our experimental results lead to the conclusion that (i) deprotonated adenine radicals are produced in equal concentration to that of the hydrated electrons, (ii) the deprotonation of radical cations occurs before 2 μs and (iii) the transient absorption spectra below 330 nm contain the fingerprint of the dimeric reaction intermediates formed in the singlet excited state.

In contrast to one-photon ionization, the survival probability of deprotonated adenine radicals in the duplexes does depend on the base sequence, with their half life being significantly longer in the homopolymeric duplex (4 ± 1 ms) than in the alternating (2.0 ± 0.1 ms) duplex. We have correlated this difference with the larger amplitude of conformational motions in the alternating structure, which could increase the probability of reaching configurations favouring radical reactivity. In order to confirm this hypothesis, both identification of the reaction products and molecular dynamics simulations are needed. However, it is also possible that the radical reaction products in the homopolymeric duplexes are different to those in the alternating duplexes.

The computed reaction pathways on the singlet excited states explained why the formation of the TA* photoproduct, isolated half a century ago, is less probable within double stranded structures.[21] More importantly, analysis of the potential energy surfaces, in combination with the computed and experimental absorption spectra, identified a reaction intermediate, which could be the precursor of the most abundant "adenine–thymine" photo-dimer formed in duplexes.[24]

Finally, our experimental spectra show that adenine radicals give rise to a reaction product characterized by an absorption band that peaks at around 350 nm, that is at a longer wavelength compared to that of other photoproducts. We hope that this spectral identification will help in the determination of its chemical structure.

Acknowledgements

Financial support from the French National Research Agency (ANR-12-BS08-0001-01, OPHID project), the CNRS-CNR PICS project (No. 6827-2015)/Bilateral CNR/

CNRS and the Université Paris-Saclay (Chaire d'Alembert No. 2016-10751) is acknowledged.

References

1 J. Cadet, A. Grand and T. Douki, in *Photoinduced Phenomena in Nucleic Acids II: DNA Fragments and Phenomenological Aspects*, ed. M. Barbatti, A. C. Borin and S. Ullrich, 2015, vol. 356, pp. 249–275.
2 J. Cadet, J. R. Wagner, V. Shafirovich and N. E. Geacintov, *Int. J. Radiat. Biol.*, 2014, **90**, 423–432.
3 C. A. Schroeder, E. Pluharova, R. Seidel, W. P. Schroeder, M. Faubel, P. Slavicek, B. Winter, P. Jungwirth and S. E. Bradforth, *J. Am. Chem. Soc.*, 2015, **137**, 201–209.
4 M. Gomez-Mendoza, A. Banyasz, T. Douki, D. Markovitsi and J. L. Ravanat, *J. Phys. Chem. Lett.*, 2016, **7**, 3945–3948.
5 J. Cadet and P. Vigny, in *Bioorganic Photochemistry*, ed. H. Morrison, John Wiley & Sons, New York, 1990, pp. 1–272.
6 T. Mohammad and H. Morrison, *J. Am. Chem. Soc.*, 1996, **118**, 1221–1222.
7 C. E. Crespo-Hernández and R. Arce, *Photochem. Photobiol.*, 2002, **76**, 259–267.
8 S. Marguet, D. Markovitsi and F. Talbot, *J. Phys. Chem. B*, 2006, **110**, 11037–11039.
9 V. Gabelica, F. Rosu, E. De Pauw, R. Antoine, T. Tabarin, M. Broyer and P. Dugourd, *J. Am. Soc. Mass Spectrom.*, 2007, **18**, 1990–2000.
10 L. P. Candeias and S. Steenken, *J. Phys. Chem.*, 1992, **96**, 937–944.
11 F. Torche and J. L. Marignier, *J. Phys. Chem. B*, 2016, **120**, 7201–7206.
12 R. Arce, *Photochem. Photobiol.*, 1987, **45**, 713–722.
13 L. P. Candeias and S. Steenken, *J. Am. Chem. Soc.*, 1992, **114**, 699–704.
14 S. Marguet and D. Markovitsi, *J. Am. Chem. Soc.*, 2005, **127**, 5780–5781.
15 A. Banyasz, L. Martinez-Fernandez, T. Ketola, A. Muñoz-Losa, L. Esposito, D. Markovitsi and R. Improta, *J. Phys. Chem. Lett.*, 2016, **7**, 2020–2023.
16 Y. Rokhlenko, J. Cadet, N. E. Geacintov and V. Shafirovich, *J. Am. Chem. Soc.*, 2014, **136**, 5956–5962.
17 A. Banyasz, T. Ketola, A. Muñoz-Losa, S. Rishi, A. Adhikary, M. D. Sevilla, L. Martinez-Fernandez, R. Improrta and D. Markovitsi, *J. Phys. Chem. Lett.*, 2016, **7**, 3949–3953.
18 A. Banyasz, *et al.*, *J. Am. Chem. Soc.*, 2017, **139**(30), 10561–10568.
19 Y. Wang, R. C. Jensen and W. E. Stumph, *Nucleic Acids Res.*, 1996, **24**, 3100–3106.
20 S. N. Bose, R. J. H. Davies, S. K. Sethi and J. A. McCloskey, *Science*, 1983, **220**, 723–725.
21 S. N. Bose, S. Kumar, R. J. H. Davies, S. K. Sethi and J. A. McCloskey, *Nucleic Acids Res.*, 1984, **12**, 7929–7947.
22 X. D. Zhao, S. Nadji, J. L. F. Kao and J. S. Taylor, *Nucleic Acids Res.*, 1996, **24**, 1554–1560.
23 R. J. H. Davies, J. F. Malone, Y. Gan, C. J. Cardin, M. P. H. Lee and S. Neidle, *Nucleic Acids Res.*, 2007, **35**, 1048–1053.
24 S. Asgatay, A. Martinez, S. Coantic-Castex, D. Harakat, C. Philippe, T. Douki and P. Clivio, *J. Am. Chem. Soc.*, 2010, **132**, 10260–10261.

25 C. Yoon, G. G. Prive, D. S. Goodsell and R. E. Dickerson, *Proc. Natl. Acad. Sci. U. S. A.*, 1988, **85**, 6332–6336.
26 L. Martínez-Fernández and R. Improta, *Photochem. Photobiol. Sci.*, 2017, **16**, 1277–1283.
27 Y. Zhao and D. G. Truhlar, *Acc. Chem. Res.*, 2008, **41**, 157–167.
28 Y. Zhao, N. E. Schultz and D. G. Truhlar, *J. Chem. Theory Comput.*, 2006, **2**, 364–382.
29 J. Tomasi, B. Mennucci and R. Cammi, *Chem. Rev.*, 2005, **105**, 2999–3093.
30 S. Miertus, E. Scrocco and J. Tomasi, *Chem. Phys.*, 1981, **55**, 117–129.
31 A. Banyasz, T. Douki, R. Improta, T. Gustavsson, D. Onidas, I. Vayá, M. Perron and D. Markovitsi, *J. Am. Chem. Soc.*, 2012, **134**, 14834–14845.
32 R. Improta, *J. Phys. Chem. B*, 2012, **116**, 14261–14274.
33 L. Esposito, A. Banyasz, T. Douki, M. Perron, D. Markovitsi and R. Improta, *J. Am. Chem. Soc.*, 2014, **136**, 10838–10841.
34 G. V. Buxton, C. L. Greenstock, W. P. Helman and A. B. Ross, *J. Phys. Chem. Ref. Data*, 1988, **17**, 513–886.
35 W. M. Kwok, C. S. Ma and D. L. Phillips, *J. Phys. Chem. B*, 2009, **113**, 11527–11534.
36 Y. Zhang, K. de La Harpe, A. A. Beckstead, R. Improta and B. Kohler, *J. Am. Chem. Soc.*, 2015, **137**, 7059–7062.
37 I. Vayá, J. Brazard, M. Huix-Rotllant, A. Thazhathveetil, F. Lewis, T. Gustavsson, I. Burghardt, R. Improta and D. Markovitsi, *Chem.–Eur. J.*, 2016, **22**, 4904–4914.
38 K. L. Stevenson, G. A. Papandonakis and P. R. LeBreton, *J. Photochem. Photobiol., A*, 2000, **133**, 159–167.
39 K. Kobayashi, *J. Phys. Chem. B*, 2010, **114**, 5600–5604.
40 L. D. Wu, K. H. Liu, J. L. Jie, D. Song and H. M. Su, *J. Am. Chem. Soc.*, 2015, **137**, 259–266.
41 B. Bouvier, T. Gustavsson, D. Markovitsi and P. Millié, *Chem. Phys.*, 2002, **275**, 75–92.
42 B. Bouvier, J. P. Dognon, R. Lavery, D. Markovitsi, P. Millié, D. Onidas and K. Zakrzewska, *J. Phys. Chem. B*, 2003, **107**, 13512–13522.
43 C. von Sonntag, *Free-Radical-Induced DNA damage and its Repair*, Springer-Verlag, Berlin-Heildelberg, 2006.
44 S. Kumar, N. D. Sharma, R. J. H. Davies, D. W. Phillipson and J. A. McCloskey, *Nucleic Acids Res.*, 1987, **15**, 1199–1216.
45 S. Kumar, P. C. Joshi, N. D. Sharma, S. N. Bose, R. J. H. Davies, N. Takeda and J. A. McCloskey, *Nucleic Acids Res.*, 1991, **19**, 2841–2847.
46 R. Improta, V. Barone, G. Scalmani and M. J. Frisch, *J. Chem. Phys.*, 2006, **125**, 054103.
47 D. B. Bucher, B. M. Pilles, T. Carell and W. Zinth, *Proc. Natl. Acad. Sci. U. S. A.*, 2014, **111**, 4369–4374.